Understanding the CVD process of (Si)–B–C ceramics through FTIR spectroscopy gas phase analysis

Jérôme Berjonneau, Francis Langlais, Georges Chollon

▶ **To cite this version:**

Jérôme Berjonneau, Francis Langlais, Georges Chollon. Understanding the CVD process of (Si)–B–C ceramics through FTIR spectroscopy gas phase analysis. Surface and Coatings Technology, 2007, 201 (16-17), pp.7273-7285. 10.1016/j.surfcoat.2007.01.039 . hal-02326650

HAL Id: hal-02326650
https://hal.science/hal-02326650

Submitted on 31 Oct 2019

HAL is a multi-disciplinary open access archive for the deposit and dissemination of scientific research documents, whether they are published or not. The documents may come from teaching and research institutions in France or abroad, or from public or private research centers.

L'archive ouverte pluridisciplinaire **HAL**, est destinée au dépôt et à la diffusion de documents scientifiques de niveau recherche, publiés ou non, émanant des établissements d'enseignement et de recherche français ou étrangers, des laboratoires publics ou privés.

Available at: https://doi.org/10.1016/j.surfcoat.2007.01.039

Understanding the CVD process of (Si)-B-C ceramics through FTIR spectroscopy gas phase analysis

J. Berjonneau, F. Langlais* and G. Chollon

Laboratoire des Composites Thermostructuraux,
UMR 5801 : CNRS - Snecma - CEA - UB1,
3 Allée de la Boétie, 33600 Pessac, France

Abstract – B-C and Si-B-C ceramics are used as self-healing matrices in ceramic matrix composites. They can be processed by CVD respectively from BCl_3-CH_4-H_2 and BCl_3-CH_3SiCl_3-H_2 precursors under reduced pressure and relatively low temperature. An investigation of the CVD process is presented for the two systems on the basis of a FTIR in situ analysis of the gas phase. By adding a porous substrate with a high internal surface in the hot zone of the reactor, the consumption of specific species is enhanced, revealing the effective precursors of the solid (e.g., $HBCl_2$ giving rise to boron). In order to better understand the mechanisms of the solid formation, correlations are pointed out between the gas phase analysis, the deposition kinetics and the properties of the coatings. In the B-C system, an amorphous carbon-rich boron carbide (comprising mostly B-C bonds) is obtained according to a heterogeneous reaction between $HBCl_2$ and a carbon effective precursor (e.g. the $CH_3^{\bullet}$ radical), the C content of the coating increasing with the maturation of the hydrocarbon (i.e. with increasing temperature and P_{CH_4}). In the Si-B-C system, two chemical processes compete against each other. The first one, occurring at low temperature (800-900°C), is similar to that involved for the B-C system. The second one, gradually prevailing at higher temperature (900-1000°C), is governed by the formation of Si-C bonds according to a heterogeneous reaction between hydrocarbons and chlorosilanes. This process competes with the formation of B-C bonds and gives rise to SiC nanocrystals for the highest temperatures (T > 1000°C), in a kinetic regime controlled by the mass transfers.

* Corresponding author : langlais@lcts.u-bordeaux1.fr

Keywords: CVD; (Si)-B-C; Gas phase analysis; FTIR; Deposition process

1- INTRODUCTION

The durability of SiC-based ceramic matrix composites (CMCs) under harsh conditions (mechanical stress, oxydizing environment, high temperature) can be improved by adding boron to the SiC-matrix. Its oxidation indeed leads to borosilicate glasses with a low melting point allowing crack healing between 500 and 1000°C [1-3]. A very convenient technique to process boron-based ceramic matrices is chemical vapour infiltration (CVI). The ternary ceramic Si-B-C can be infiltrated from the BCl_3-CH_3SiCl_3(MTS)-H_2 gaseous precursor. Due to the complexity of this system, the study of the deposition of B-C ceramics (which are also used in self-healing matrices) from the BCl_3-CH_4-H_2 precursor is a helpful preliminary approach. The CVD of the B-C system has furthermore been widely investigated through theoretical and experimental approaches [4-14]. Conversely, except for the work of Goujard et al., very few studies have been carried out on the CVD of the Si-B-C ternary system [1-3, 15-17].

In order to control and optimize the processing of B-C and Si-B-C ceramic matrices and build an overall modelling of the CVI processes, it is necessary to identify the CVD kinetics and deposition mechanisms. The infiltration of a ceramic within fibrous performs requires to promote mass transfer with respect to chemical reaction rates. A hot-wall reactor operating at low temperature and reduced pressure is therefore preferred [18]. Except for the studies of Hannache et al. in the B-C system and Goujard et al. in the Si-B-C system, such conditions were not explored in the previous works. For the former system, most of the investigations were carried out using cold wall reactors at relatively high temperature (T > 1000°C) and either at atmospheric or reduced pressure. Vandenbulcke et al. proposed mass transfer-equilibrium and mass transfer-kinetics models and compared the theoretical data to the experimental deposition rates. These authors evidenced the limiting kinetic effect of the carbon formation from the decomposition of CH_4, especially at low temperature, giving rise to carbon-rich rhombohedral ($B_{13}C$ or $B_{13}C_3$) and amorphous (BC_x) boron carbide. These results were later confirmed by Jansson et al. [10], who pointed out the difficulty to obtain a high carbon content in the films deposited under reduced pressure ($x_c < 22$ at.% for $1 < P < 7$ kPa). In the case of the Si-B-C system, the temperatures and pressures explored by Goujard et al. [16] or Golda and Gallois [17] are relatively high (e.g., P = 40 or 30 kPa, respectively) and

not favourable to an effective infiltration process. Furthermore, the data obtained by these authors are incomplete to satisfactorily determine the kinetic laws of deposition (activation energies and partial reaction orders were not determined) and the homogeneous reactions involved in the process.

As recently shown in the case of laminar pyrocarbon deposition, a multiple experimental investigation (including in particular a kinetic study, a physico-chemical characterization and a gas phase analysis) is helpful to understand the CVD mechanisms [19]. The same approach has been very recently applied to the CVD of B-C and Si-B-C ceramics [20, 21]. In both cases, the results of the various experimental approaches were correlated and have supported preliminary discussions on the chemical processes respectively involved. The purpose of the present contribution is to emphasize the in-situ gas phase analysis, by mean of the FTIR spectroscopy. This technique has been shown to be very fruitful to identify, sometimes in conjunction with a thermodynamic study, the intermediate species playing the role of the effective precursors of the solid deposited, e.g. pyrocarbon [19], diamond [22], silicon [23], silicon carbide [24-26], boron carbide [8] and various oxides SnO_2[27], $BaSrTiO_3$ [28], Pb (Zr, Ti) O_3 [29]. For the present study of both the B-C and Si-B-C systems, correlations are reported between (1) in-situ FTIR gas phase analysis, (2) characterization of the coatings, (3) kinetic study and, as a conclusion, the various chemical processes possibly involved are discussed.

2- EXPERIMENTAL

2.1- CVD equipment

The B-C and Si-B-C ceramics were deposited on dense and polished graphite cylindrical substrates (10 mm height, 10 mm diameter) in a low pressure hot-wall CVD reactor (Fig. 1). This reactor is a vertical silica glass tube (700 mm length, 34 mm internal diameter) heated in its central part by a radio-frequency induction furnace using a 130 mm long graphite susceptor including a K-type thermocouple. The isothermal zone is 100 mm high within a temperature range of (T ± 25°C). The reactor is fed downward with the various species of the precursor mixture through electronic mass flow controllers (from Brooks Instruments) regulating the partial flow rates Q_i. The effluent gases are pumped via cold traps by a classical rotary pump (from Alcatel). The total pressure P is controlled with a motorized valve coupled to a variable capacitance pressure gauge (both form MKS Instruments).

2.2- FTIR in-situ analysis

For the gas phase analysis, a FTIR spectrometer (Nicolet 550) was coupled to the CVD reactor (Fig. 1). The infrared beam coming out of the optical bench of the spectrometer is directed towards the entrance window (ZnSe) with a mirror. The parallel beam passes axially through the reactor, integrating signals due to the precursor and the various species produced in the hot reaction zone. The output IR beam is directed to and focused on a HgCdTe (MCT-A) detector cooled by liquid nitrogen. The mirrors and detector outside the optical bench and the tubing confining the whole IR-beam are purged with a nitrogen flow to prevent absorption by atmospheric water and carbon dioxide.

The variations of the gas phase composition were studied by infrared absorption spectroscopy, which provides a rapid measurement of the relative amounts of the detected species. For each absorption spectrum, about one hundred scans were collected in a spectral range from 600 to 4000 cm^{-1} and with a spectral resolution of 1 cm^{-1}. The background spectrum was collected just before the sample spectrum by replacing the precursor mixture by a pure hydrogen flow at the same temperature. The relative concentrations of the various identified molecules were estimated by measuring the areas of representative peaks on the spectra displaying the absorbance versus wave number. A linear dependence between peak area and concentration can be assumed because of the low partial pressures (Beer-Lambert law). For each condition, three spectra were recorded in order to reduce the experimental errors.

Moreover, an annular porous carbon substrate with a high specific area and allowing the IR beam to go through, was in a few cases added in the hot zone, to more specifically favour the heterogeneous reactions and identify the consumed species.

2.3- CVD conditions

For both the B-C and Si-B-C systems, the experimental conditions were chosen compatible with the CVI process. The total pressure was P = 2, 5 and 12 kPa. The temperature T ranged from 750 to 1050°C. The total flow rate Q was chosen in the range 50-500 sccm. The initial gas phase composition was defined by the ratios $\delta = P_{BCl_3}/P_{CH_4}$ and $\gamma = P_{H_2}/P_{BCl_3}$, for the B-C system and $\alpha = P_{H_2}/P_{MTS}$ and $\beta = P_{MTS}/P_{BCl_3}$, for the Si-B-C system. The initial

composition ranges were chosen as follows, for the B-C system: $2 < \delta = P_{BCl3}/P_{CH4} < 4$ and $2 < \gamma = P_{H2}/P_{BCl3} < 5$ i.e., with a large excess of hydrogen to promote the reduction of BCl_3 and a slight excess of BCl_3 with respect to CH_4, to adjust the stoichiometry of boron carbide (Fig. 2) and for the Si-B-C system: $12 < \alpha = P_{H2}/P_{MTS} < 20$ and $0.3 < \beta = P_{MTS}/P_{BCl3} < 1$ resulting, besides the large excess of H_2, to a slight excess of BCl_3 with respect to MTS to obtain boron-rich Si-B-C ceramics (Fig. 3).

3- RESULTS

3.1- B-C ceramics from BCl_3-CH_4-H_2

The main gaseous species detected in situ by FTIR spectrometry were BCl_3, $HBCl_2$ and HCl, as shown in the typical spectrum of figure 4. The positions of the characteristic bands and the associated vibration modes are given in table 1. The peak areas are represented in figures 5 and 6 as a function of temperature, for the four limit compositions of the studied domain at P = 12 kPa and for $\delta = 4$, $\gamma = 5$ at P = 2 kPa, either in the presence or without porous perform in the hot zone. Owing to the contribution of the inlet initial species in the upper part of the reactor and the outlet gases (products and unreacted species) in the lower part, the variations of the IR peak areas characteristic of the reactants (CH_4, BCl_3) versus temperature are therefore underestimated with respect to the variations of the intermediate species such as $HBCl_2$. The slight decrease of the CH_4 and BCl_3 apparent concentrations when the temperature increases up to 500°C, can be explained by a thermal expansion of the gases (their decomposition is not expected in this temperature range [20]). This decrease is enhanced when the temperature rises above 500°C, in qualitative agreement with the homogeneous equilibrium recently calculated (Fig. 7) [20]. The initiation of the consumption of BCl_3 at low temperature is directly related to the starting production of $HBCl_2$ and HCl according to the reaction:

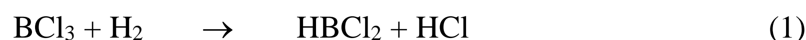

$$BCl_3 + H_2 \rightarrow HBCl_2 + HCl \quad (1)$$

This result is in agreement with the FTIR analyses carried out by Noyan Dilek et al. [8] for the CVD on a tungsten substrate from the same BCl_3-CH_4-H_2 system, at atmospheric pressure and

high temperature (between 1200 and 1450°C) and for slightly higher initial concentration of BCl_3 (2.5 < δ < 6). These authors have shown the presence of $HBCl_2$ in the reactor for a temperature as low as 350°C. Moreover, such a species had already been evidenced by FTIR for the BCl_3-H_2 system [33-35] and by mass spectrometry for the BCl_3-$TiCl_4$-H_2 system [36-37].

Considering now the carbon source species, the dehydrogenation of CH_4 into C_2H_2, according to the reaction:

$$2\,CH_4 \rightarrow C_2H_2 + 3\,H_2 \qquad (2)$$

which was predicted by the homogeneous equilibrium calculation (Fig. 7), is not detected in the present in-situ FTIR analysis. This is probably due to a fast heterogeneous consumption of this reactive hydrocarbon, as opposed to its slow homogeneous production.

The peak area of $HBCl_2$ exhibits a maximum at about 800-900°C, corresponding to the starting deposition of the solid. $HBCl_2$ is homogeneously produced according to reaction (1) below this temperature, whereas it is partly consumed beyond 900°C, probably through both homogeneous reaction (e.g., forming further reduced species such as H_2BCl, as shown in figure 7) and heterogeneous reaction with a hydrocarbon, to produced boron carbide.

The various reactions described above are enhanced by the addition of a porous substrate in the hot zone of the reactor. Only homogeneous reactions take place below 800°C (e.g., reaction (1)), the deposition rate being indeed negligible [20], whereas both the homogeneous and heterogeneous reactions are expected to occur above 800°C. The addition of a porous substrate gives rise to a further consumption of CH_4 and $HBCl_2$, but only at temperatures beyond 800°C, corresponding to the starting of the solid deposition. Both species can therefore be assumed to contribute rather directly to the heterogeneous process (Fig. 5). It can be noticed that when the temperature increases up to the highest investigated values (i.e. 1000-1050°C) and for the total pressure of 12 kPa, the consumption of CH_4 is apparently enhanced whereas that of $HBCl_2$ tends to be reduced. This change of the gas phase may be associated with a decrease of the B/C atomic ratio at high temperature. On the other hand, when δ decreases from 4 to 2 (i.e. when P_{CH4} increases, as shown in figure 2), the consumption of $HBCl_2$ increases (Fig. 5) indicating the role of CH_4 in promoting the deposition process. This phenomenon should lead to a boron-enriched coating and a higher deposition rate as δ decreases. HCl is produced in higher amounts as the temperature is raised and in presence of a porous substrate. This results from (i) the homogeneous reaction (1),

corresponding to the formation of $HBCl_2$ at temperatures lower than 800°C and (ii) both homogeneous and heterogeneous reactions, giving rise to boron carbide beyond 800°C.

For a pressure of 2 kPa and an initial composition given by $\delta = 4$, $\gamma = 5$, the thermal behaviours of the peak areas are similar to those observed at 12 kPa, except for $HBCl_2$ (Fig. 6). The concentration of this species in the presence of a porous substrate remains higher than that without substrate over almost the whole temperature range (i.e. up to 1000°C). This result shows that $HBCl_2$, which is only slightly produced by reaction (1), is not significantly consumed through heterogeneous reactions, probably owing to the very low partial pressure of CH_4 (0.08 kPa). To be more thoroughly understood, this specific result must be correlated with a kinetic study and a characterization of the deposit.

The present FTIR gas phase analysis of the BCl_3-CH_4-H_2 system experimentally establishes the role of $HBCl_2$ as a reactional intermediate in the deposition process of boron carbide, provided a sufficient pressure ($P > 10$ kPa). This result is consistent with that obtained by Noyan Dilek et al. for slightly different conditions[8].

3.2- Si-B-C ceramics from BCl_3-CH_3SiCl_3-H_2

A typical IR spectrum of the gas phase in the BCl_3-CH_3SiCl_3-H_2 system (for T = 900°C, P = 12 kPa, $\alpha = 12$, $\beta = 1$ and Q = 420 sccm) is shown in figure 8. The gaseous species detected are MTS, $SiCl_4$, chlorosilanes H_xSiCl_{4-x} (with x = 1, 2, 3), CH_4, BCl_3, $HBCl_2$ and HCl. The position of the characteristic bands chosen for the analysis and their corresponding vibration modes are given in table 2. The assignment of the peaks associated to MTS and its derived species was carried out on the basis of previous studies on the CVD/CVI of SiC ceramics from MTS/H_2 precursor [24-26]. The analysis of BCl_3 and $HBCl_2$ was based on the present investigation on the B-C system.

The peak areas are represented in figure 9 as a function of temperature (from room temperature to 1050°C) for P = 12 kPa, $\alpha = 12$ and $\beta = 1$, either in the presence or without annular porous substrate in the reactional zone. From room temperature to about 500°C, the peak areas of MTS and BCl_3 both slightly decrease owing, as for the B-C system, to the thermal expansion of the gases. The decrease becomes much more significant as the temperature rises, from about 800°C for MTS and 600°C for BCl_3. As for the B-C system, the starting consumption of BCl_3 at low temperature is directly related to the production of $HBCl_2$ and HCl through homogeneous reactions (Fig. 9e-9g). Similarly, the consumption of MTS is

associated with the production of $SiCl_4$, H_xSiCl_{4-x} and CH_4 (Fig. 9a-9d). The decomposition of BCl_3 is strongly enhanced by the addition of a porous substrate (starting at 400°C instead of 600°C). At such a low temperature, the deposition rate is negligible and heterogeneous reactions are not expected to occur. The porous substrate can be assumed to favour the homogeneous reactions (e.g. the reduction of BCl_3 into $HBCl_2$) by increasing the effective residence time of the gas phase in the hot zone. Conversely, the decomposition of MTS is only slightly enhanced by the porous substrate (starting at 750°C instead of 800°C, Fig. 9a). As already observed for the B-C system, the $HBCl_2$ peak area exhibits a maximum at about 850-900°C without substrate and 750°C with the substrate (Fig. 9f), corresponding to the starting deposition of the solid[20]. Below these temperatures, $HBCl_2$ is homogeneously produced whereas beyond, it is partly heterogeneously consumed to form B-C bonds through a reaction with a hydrocarbon. For the highest temperatures ($T > 850$°C), the peak area drop induced by the porous substrate can be assigned mostly to the heterogeneous consumption of $HBCl_2$ and should be therefore related to the boron content of the coating. The peak areas of CH_4 and the chlorosilane species show a maximum at about 1000°C, either in presence or without porous substrate (Fig. 9b-9d). A heterogeneous consumption of these species (as shown by the peak area drop due to the porous substrate) is however observed to increase with temperature from 900 to 1050°C, which may give rise to an increase of the silicon and carbon contents in the coating.

Figure 10 shows the peak areas of $SiCl_4$ and chlorosilanes H_xSiCl_{4-x} versus temperature at $P = 12$ kPa and $\alpha = 20$, $\beta = 0.3$. The influence of the gas phase initial composition on the heterogeneous consumption of the MTS-derived species can be assessed by comparison with Figure 9b-9c. When the composition varies from $\alpha = 12$, $\beta = 1$ to $\alpha = 20$, $\beta = 0.3$ (i.e., when the MTS partial pressure decreases from 0.86 to 0.49 kPa, hindering its decomposition), a strong decrease of the consumption of $SiCl_4$ and chlorosilanes is observed, suggesting a possible decrease of the silicon content in the coating.

The increase of the total flow rate (i.e. the decrease of the residence time) results in a decrease of the heterogeneous consumption of $HBCl_2$ (Fig. 11) which may induce a decrease of the boron content in the coating.

Finally, the gas phase composition at $P = 5$ kPa, $\alpha = 12$ and $\beta = 1$ was compared to the same condition but in the absence of BCl_3 in the initial gas mixture ($P = 5$ kPa, $\alpha = 12$), with a view to investigate the role of BCl_3 in the decomposition of MTS. The production of $SiCl_4$ is strongly enhanced by the presence of BCl_3, whereas the formation of CH_4 is almost

unaffected (Fig. 12). The small influence of BCl_3 on the CH_4 concentration could be explained by a heterogeneous consumption of CH_4 (or of its direct precursor the radical $CH_3^{\bullet}$), within the low temperature range ($780 < T < 900$°C), counterbalancing its homogeneous production from the decomposition of MTS. This phenomenon would then result in a high carbon content in the deposit.

The present FTIR investigation of the gas phase in the BCl_3-MTS-H_2 system suggests the existence of two parallel routes in the deposition of Si-B-C ceramics : the first one resulting in the formation of boron from $HBCl_2$, at relatively low temperature (from about 800°C) ; the second one giving rise to the formation of silicon from chlorosilane at higher temperatures (from about 900°C).

4- DISCUSSION AND CONCLUSIONS

4.1- Previous results on the deposition kinetics and the properties of the coatings

4.1.1- B-C ceramics from BCl_3-CH_4-H_2[20]

A kinetic study was carried out to define a domain of experimental conditions where the process is limited by the chemical reactions (characterized by linear Arrhenius plots and deposition rates independent of the total flow rate). The Arrhenius plots LnR = f(1000/T) reported in figure 13 for the total pressure of 12 kPa and the four initial compositions previously defined (conditions (1) to (4), given in figure 2) show linear behaviours between 800 and 975°C. The apparent activation energies and the reaction orders with respect to the initial gaseous species (BCl_3, CH_4, H_2) were derived within these domains. This allowed to propose the following general kinetic law $R = R_o \exp(-E_a/RT)\, P_{CH4}\, P_{BCl3}^{-0.5}$, valid for a total pressure close to 12 kPa, where R_o and E_a depend on the initial composition and the temperature range (table 3). For a specific condition of pressure and initial composition (P = 2 kPa and $\delta = 4$, $\gamma = 5$), a singular kinetic behaviour was observed, characterized by the absence of a linear domain in the Arrhenius plot (Fig. 14).

For the initial compositions (1) to (4), a pressure of 12 kPa, and for temperatures and total gas flow rates chosen within the kinetic domain controlled by chemical reactions, the B/C atomic ratio ranges from 2 to 3.5, indicating a carbon excess with respect to the

stoichiometry of B_4C (table 4). This ratio was found to decrease when the deposition temperature increases and more specifically between 950 and 1000°C, for $\delta = 2$, $\gamma = 5$. The surface and fracture section morphology was homogeneous and amorphous-like for the low temperature coatings and exhibited an extremely fine nanotexture for the samples processed at the highest temperatures. XRD could not evidence any organized phase. The occurrence of crystalline boron carbide and free aromatic carbon (with a sp^2 hybridization) was not even revealed by Raman microspectroscopy. For the condition P = 2 kPa, $\delta = 4$, $\gamma = 5$, related to the singular Arrhenius plot shown in Fig. 14, the coatings contained a high concentration of boron at 800°C (atomic ratio B/C > 4) and carbon at 1000°C (B/C << 1).

4.1.2- Si-B-C ceramics from BCl_3-CH_3SiCl_3-H_2 [21]

For this more complex system, a large experimental domain favourable to a kinetic process limited by the chemical reactions has been evidenced. The deposition rate does not depend on the total flow rate over the whole investigated domain except for P = 12 kPa and an initial composition not too rich in H_2 ($\alpha = 12$). The Arrhenius plots (Fig. 15) have revealed a linear behaviour over the whole studied temperature range at 2 kPa and for T < 1000°C at 5 and 12 kPa. At P = 2 kPa, a single kinetic regime was observed with an apparent activation energy of about 185 $kJmol^{-1}$. At P = 5 and 12 kPa, two chemical regimes were evidenced : the first one for intermediate temperatures (900 < T < 1000°C), with an apparent activation energy close to 285 $kJmol^{-1}$ and the second one at lower temperature (T < 900°C), with a lower activation energy of about 180 $kJmol^{-1}$. At 12 kPa, for $\alpha = 12$ and $\beta = 1$, a decrease of the total flow rate from 420 to 175 sccm results in a noticeable increase of the deposition rate (Fig. 15c). Such a transition between two chemical processes, characterized by an increase of the activation energy with temperature, suggests a competition between two parallel deposition routes, the fastest prevailing over the slowest one. The determination of the apparent reactions orders at 800 and 900°C for P = 12 kPa confirmed and more precisely defined the transition between the two distinct kinetic regimes. The reaction order with respect to MTS is positive and relatively high (0.8 at 800°C and 1.6 at 900°C). Conversely, the reaction order with respect to BCl_3 is slightly negative (-0.2 at 800°C and -1.5 at 900°C). As in the case of the B-C system, these negative reaction orders can be related to an inhibition effect due to the HCl species produced by the homogeneous decomposition of BCl_3. This was

confirmed by the highly negative value of the reaction order with respect to HCl, at high HCl partial pressures (-2.5 at 800°C and -4.2 at 900°C).

The Si, B and C atomic concentrations of the coatings were determined by AES for temperatures ranging from 750 to 1050°C, for three different pressures 2, 5 and 12 kPa and for two gas phase compositions $\alpha = 12$, $\beta = 1$ and $\alpha = 20$, $\beta = 0.3$ (Fig. 16). The Si atomic concentration is surprisingly low, ranging from 0.5 to 18%, the C content ranges from 23 to 42 at. % and the B content remains relatively high (from 40 to 75 at. %). The Si concentration increases when both the temperature and the MTS and H_2 initial contents increase with respect to BCl_3. The variations of the B concentration exhibit a maximum while those of C show a minimum around 900°C. These changes in the B and C contents together with the increase of the Si content (especially beyond 900°C) can be related to the kinetic transition evidenced above, in terms of activation energy and MTS reaction order. The morphology of the coatings obtained at low temperature was found homogeneous and amorphous-like while an extremely fine nanotexture was observed for the solid deposited at the highest temperatures. When the temperature increases and the MTS and H_2 initial partial pressures both increase with respect to BCl_3, β–SiC nanograins are formed within an amorphous phase (possibly consisting of B_xC_y icosahedra units with a high C content, but not containing any sp^2 or sp^3 free carbon phase), as shown by Raman microspectroscopy, X-ray diffraction and TEM analyses.

4.2- Correlations

The first significant conclusion of the present multiple experimental work on the deposition of both B-C and Si-B-C systems is the role of $HBCl_2$ as an intermediate species for the *formation of boron* in the deposit. This conclusion is supported in particular by the correlation between (i) the consumption of $HBCl_2$ in the presence of a porous substrate, decreasing at high temperature (T > 1000°C) (Fig. 5 and 9) and (ii) the decrease of the boron content in the solid (in both B-C and Si-B-C coatings) (Table 4 and Fig. 16). At low temperature (T < 800°C), $HBCl_2$ is only produced by homogeneous decomposition of BCl_3 (enhanced by the presence of a porous substrate). For intermediate temperatures (800 < T < 1000°C), a competition occurs between the homogeneous formation and the consumption of $HBCl_2$, resulting in a maximum of concentration within this temperature range (Fig. 5 and 9). In the Si-B-C system, the change in the kinetic regime at about 900°C (Fig. 15) can be related to the maximum of the B content in the coating (Fig. 16) and to the maximum of $HBCl_2$

consumption in the presence of a porous substrate (Fig. 9). The importance of the $HBCl_2$ species is also evidenced in Fig. 11. The decrease of the total flow rate indeed favours the consumption of $HBCl_2$, resulting in an increase of both the deposition rate (Fig. 15c) and the boron content (Fig. 16), the major element of the Si-B-C coating.

The effective precursor responsible for the *formation of carbon* in both systems, is less clearly evidenced. For B-C coatings, C_2H_2 is a possible reactional intermediate which might be readily decomposed into carbon after being produced by the dehydrogenation of methane (though this process is not experimentally established). When P_{CH4} is increased (e.g., by decreasing δ from 4 to 2, as shown in Fig. 5), the consumption of $HBCl_2$ and to a lesser extent of CH_4 are increased, resulting in (i) a higher deposition rate (as shown by the Arrhenius plots of Fig. 13 and the reaction orders, especially with respect to CH_4) and (ii) a boron-enriched coating (as reported for several conditions in Table 4). For Si-B-C coatings, the carbon and silicon effective precursors both result from the decomposition of MTS in the presence of H_2. The FTIR analysis identified CH_4 and chlorosilanes (including $SiCl_4$) as respective intermediates in the formation of carbon and silicon. Their consumption (mainly heterogeneous) increases with temperature from 900 to 1050°C and correspond to an increase of the carbon and silicon contents in the coating. The effective precursor of carbon is probably the radical $CH_3^{\bullet}$ resulting from the decomposition of MTS. Due to the high reactivity at low temperatures of the effective boron precursor $HBCl_2$, the effective carbon precursor is more likely to react with $HBCl_2$ than with the silicon precursors, giving rise to B-C rather than Si-C bonds. This process can explain the increase of the production of $SiCl_4$ when BCl_3 is added to MTS/H_2 (Fig. 12). The decomposition of MTS (favoured by this addition) produces (i) $SiCl_4$ (and more generally chlorosilanes), remaining in the gas phase and (ii) $CH_3^{\bullet}$ quickly reacting with $HBCl_2$ to form B-C bonds in the solid. This may also explain the relatively high carbon content in the Si-B-C deposit (> 23 at. %).

The *formation of silicon* during the Si-B-C deposition process occurs through a chlorosilane as effective precursor, but at a temperature higher than that required for the formation of boron. The consumption of chlorosilanes is indeed effective beyond 850 – 900°C (Fig. 9), where significant amounts of Si are formed (Fig. 16). This consumption of chlorosilanes, enhanced by increasing temperature and directly associated with the Si content of the coating, is also favoured by increasing the MTS partial pressure (e.g. from $\alpha = 20$, $\beta = 0.3$ to $\alpha = 12$, $\beta = 1$).

4.3- Conclusions on the deposition mechanisms

Within the experimental conditions explored in the present contribution, the solid deposited from the BCl_3-CH_4-H_2 precursor is an amorphous boron carbide enriched in carbon with respect to the stoichiometry of the crystallized forms existing in the B-C system. The B/C atomic ratio ranges from 2 to 3.6, depending on the temperature and the CH_4 initial partial pressure. In the deposition mechanism, the most influential step is the heterogeneous reaction between $HBCl_2$ and the carbon effective precursor. This carbon precursor, which is fundamental in the process, is a hydrocarbon with a certain degree of maturation (i.e., of dehydrogenation, as already described in studies on the deposition of pyrocarbon [19]). A higher maturation (involving a more complex chemical route) is obtained by increasing the temperature and the CH_4 initial partial pressure, resulting in higher deposition rates (i.e., a positive reaction order with respect to CH_4 and an increase of the activation energy with P_{CH_4}) and finally in carbon-enriched coatings. The mechanism involved for lower pressures (total pressure and partial pressure of CH_4) seems to be drastically influenced by temperature (see 3.1 and 4.1.1), the composition of the coating varying from boron-rich to almost pure carbon. This specific behaviour needs more investigation to be confirmed and understood.

Three main kinetic regimes can be evidenced in the CVD of Si-B-C coatings from MTS-BCl_3-H_2 precursor, depending on the temperature range. At low temperatures (800-900°C) and medium temperatures (900-1000°C), two kinetic regimes compete each other. The first one, prevailing at low temperatures is rather similar to the regime observed for the B-C system, with kinetics controlled by heterogeneous reactions between effective precursors (e.g. $CH_3^\bullet$ and $HBCl_2$) and giving rise to B-C bonds. B-B bonds can also result from the combination of boron-containing species. The coating obtained is amorphous and organized only at a very short range (in the form of disordered icosahedra) with a B/C atomic ratio close to 2. Silicon is not detected (or only in traces) and there is no evidence of aromatic C-C bonds despite the high carbon content. The second kinetic regime, which exhibits higher activation energy and reaction order with respect to MTS, appears at medium temperatures and gives rise to a true ternary solid (with significant amounts of silicon). At this temperature range, the reactivity of the silicon-containing species, the chlorosilanes, become comparable to that of $HBCl_2$ (e.g., through the formation of $SiCl_2^\bullet$ or $SiCl_3^\bullet$ radicals). The kinetic process becomes therefore controlled by the heterogeneous reactions between hydrocarbons (e.g. $CH_3^\bullet$) and chlorosilanes, to form Si-C bonds competing with B-C bonds. This transition to a different

mechanism gives an explanation of the increase of the silicon and carbon contents and the decrease of the boron content in the coating. However, the temperature is still too low (900-1000°C) to allow the formation of crystals (e.g. β-SiC), the coating remaining totally amorphous. Finally, at higher temperatures (T > 1000°C), kinetics are controlled by mass transfer. The silicon and carbon contents increase at a level sufficient to form β-SiC nanocrystals, embedded within the amorphous carbon-rich B-C phase. Such a multiphase solid is closer than that predicted by the thermodynamic calculation (SiC + B_4C + graphite) [15]. This result can be related to the mass transfer regime favouring chemical reactions and consequently the heterogeneous equilibrium.

Acknowledgements. The authors wish to thank CNRS and SAFRAN for their financial support through a grant to J. B. They are indebted to S. Bertrand and C. Descamps from SPS for fruitful discussions.

References

1- L. Vandenbulcke, Ceram. Trans. 175 (2005) 13.
2- S. Goujard and L. Vandenbulcke, Ceram. Trans. 46 (1994) 925.
3- E. Bouillon, F. Abbe, S. Goujard, E. Pestourie, G. Habarou and B. Dambrine, Ceram. Eng. Sci. Proc. 21 [3] (2000) 459.
4- A. O. Sezer and J. I. Brand, Mater. Sci. Eng., B79 (2001) 191.
5- M. Ducarroir and C. Bernard, in Proceedings of the 5th International Conference on CVD, J.M. Blochor et al., editors, p.72, The Electrochemical Society, Pennington, NJ (1975).
6- L. Vandenbulcke, R. Herbin, M. Basutcu and J.N. Barrandon, J. Less-Common Met., 80, 7 (1981).
7- L. Vandenbulcke, Ind. Eng. Chem. Proc. Res. Dev., 24 (1985) 568.
8- S. Noyan Dilek, H. O. Ozbelge, N.A. Sezgi and T. Dogu, Ind. Eng. Chem. Res., 40, 751 (2001).
9- L. R. Newkirk, R.E. Riley, H. Sheinberg, F. A. Valencia and T. C. Wallace, in Proceedings of the 7th International Conference on CVD, T. O. Sedwick et al., editors, p. 515, The Electrochemical Society, Pennigton, NJ (1979).

10- U. Jansson, J. O. Carlsson, B. Stridh, S. Soderberg and M. Olson, Thin Solid Films, 172 (1989) 81.

11- S. Lartigue, Cuzajous, M. Nadal and G.Male, in Proceedings of the 5th European Conference on CVD, p. 413, J. O. Carlsson and J. Lindsröm, editors, Uppsala, Sweden (1985).

12- H. Hannache, F. Langlais and R. Naslain, in Proceedings of the 5th European Conference on CVD, p. 219, J. O. Carlsson and J. Lindström, editors., Uppsala, sweden (1985).

13- J. Rey, G.Male, P. Kapsa and J. L. Loubet, J. Phys. Coll. , C5/T50, (1989) 311.

14- T. S. Moss, W. J. Lackey and K. L. More, J. Am. Ceram. Soc., 81 [12], (1998) 3077.

15- S. Goujard, L. Vandenbulcke, C. Bernard, G. Blondiaux and J. L. Debrun, J. Electrochem. Soc. 141 [2] (1994) 452.

16- S. Goujard, L. Vandenbulcke and C. Bernard, J. Eur. Ceram. Soc. 15 (1995) 551.

17- E. M. Golda and B. Gallois, in: T. E. Besmann, B. M. Gallois and J. W. Warren (eds), CVD of refractory metals and ceramics II, MRS Symp. Proc. 250 (1992) 167.

18- F. Langlais in: A. Kelly and C. Zweben (eds), Comprehensive Composite Materials 26 (2000) 611.

19- F. Langlais, H. Le Poche, J. Lavenac and O. Féron, Proc. EuroCVD-15, R. A. Fischer et al. (eds), Bochum, D (Sept. 2005)

20- J. Berjonneau, G. Chollon and F. Langlais, J. Electrochem. Soc., in press.

21- J. Berjonneau, G. Chollon and F. Langlais, submitted to Thin Solid Films.

22- S. Jin, L. Bourget and E. Sevillano, Surface and Coating Technology, 68/69 (1994) 394.

23- C. Panczyk and C. G. Takoudis, Proc. 14th Int. Conf. on CVD (and EuroCVD-11), M. D. Allendorf and C. Bernard (eds), The Electrochem. Soc., Pennington (1997) 652.

24- S. Jonas, W. S. Ptak, W. Sadovski, E. Valasek and C. Paluszkiewicz, J. Electrochem. Soc., 142 [7] (1995) 2357.

25- V. Hopfe, H. Mosebach, M. Erhard and M. Meyer, J. Molecular Structure 347 (1995) 331.

26- K. Brennfleck, S. Schneweis and R. Weiss, J. Phys. IV 9 (1999) 1041.

27- V. Hopfe, D. W. Sheel, C. I. M. A. Spee, R. Tell, P. Martin, A. Beil, M. Pemble, R. Weiss, U. Vogt and W. Graehlert, Thin Solid Films 442 (2003) 60.

28- G. G. Condorelli, A. Bacri and I.L. Fragala, Chem. Mater. 14 (2002) 4307.

29- K. Nagashima, H. Funakubo, S. Saki, Y. Sawada, Y. Miura, N. Higuchi and H. Machida, Chem. Vap. Depo. 6 (2000) 311.
30- R. E. Seruby, J. R. Lacher and J. D. Park, J. Chem. Phys. 19 [3] (1951) 386.
31- O. Brieux de Mandirola and J. F. Westerkamp, Spectrochimica Acta 20 [10] (1964) 1633.
32- C. O. Bass, L. Lynds, T. Wolfram and R. E. De Wames, J. Chem. Phys. 40 [12] (1964) 3611.
33- N. A. Sezgi, T. Dogu and H. O. Ozbelge, Ind. Eng. Chem. Res. 36 (1997) 5537.
34- N. A. Sezgi, T. Dogu and H. O. Ozbelge, Chem. Eng. Sci.54 (1999) 3297.
35- N. A. Sezgi, A. Ersoy, T. Dogu and H. O. Ozbelge, Chem. Eng. Proc. 40 (2001) 525.
36- J. P. Dekker, P. J. Van der Put, J. Schoonman and H.J. Veringa, J. CVD 1 [4] (1993) 317.
37- T. H. Osterheld and M. D. Allendorf in: Covalents ceramics III, Science and Technology of Non-Oxydes, The Material Research Society 410 (1996).
38- P. Mirone and P. Chirboli, Ann. Chim. 50 (1960) 1095.
39- J. Nishizawa and H. Nihira, J. Crystal Growth 45 (1978) 82.

Table captions

Table 1: Absorption band position for the gaseous species identified by FTIR spectroscopy in the BCl_3-CH_4-H_2 system.

Table 2: Absorption band position for the gaseous species identified by FTIR spectroscopy in the BCl_3-MTS-H_2 system.

Table 3 : Activation energy (E_a) and pre-exponential factor (R_0) for the deposition kinetic laws in the BCl_3-CH_4-H_2 system.

Table 4 : B/C atomic ratio of coatings deposited in the BCl_3-CH_4-H_2 system, as measured by AES

	Observed peak-position (cm^{-1})	Rotation – vibration mode		Peak position from literature (cm^{-1})
CH_4	3113	stretching ν_{C-H}	strong rotation-vibration band in R-branch	3018 [24] near 3000 [25]
BCl_3	1900	stretching ν_{B-Cl}	overtone band of $\nu_{as\ B-Cl}$ at 956 cm^{-1}	1916 [30]
$HBCl_2$	2600	stretching ν_{B-H}	-	2625 [31] 2617 [32]
HCl	2943	stretching ν_{H-Cl}	strongest rotation-vibration band in R-branch	2895-3095 [24]

Table 1: Absorption band position for the gaseous species identified by FTIR spectroscopy in the BCl_3-CH_4-H_2 system.

	Observed peak-position (cm^{-1})	Rotation – vibration mode		Peak position from literature (cm^{-1})
MTS	1270	in-plane bending	maximum of Q-branch	1272 [24] 1270 [25]
Chlorosilanes SiH_xCl_{4-x} (x=1, 2, 3)	2259	stretching $\nu_{Si\text{-}H}$	maximum of Q-branch	2260 [24, 39] 2259 [25]
$SiCl_4$	641	asymmetric stretching $\nu_{as\ Si\text{-}Cl}$	-	620 [24, 38] 641 [25]
CH_4	1306	in-plane bending $\delta_{C\text{-}H}$	maximum of Q-branch	1305 [24] 1306 [25]
BCl_3	1900	stretching $\nu_{B\text{-}Cl}$	overtone band of $\nu_{as\ B\text{-}Cl}$	1916 [30]
$HBCl_2$	1100	asymmetric stretching $\nu_{as\ B\text{-}Cl}$	-	doublet around 1100 [32]
HCl	2943	stretching $\nu_{H\text{-}Cl}$	strongest rotation-vibration band in R-branch	2895-3095 [24]

Table 2: Absorption band position for the gaseous species identified by FTIR spectroscopy in the BCl_3-MTS-H_2 system.

	γ	δ	Q_{tot} (sccm)	ΔT (°C)	E_a (kJmol^{-1})	R_0 (µgcm^{-2}min^{-1})
①	5	4	250	825-975	260±10	8.10^{11}
②		2	390	800-975	298±8	7.10^{13}
③	2	4	390	800-900	297±10	4.10^{13}
				900-975	425±10	2.10^{19}
④		2	210	825-925	473±12	10^{22}

Table 3 : Activation energy (E_a) and pre-exponential factor (R_0) for the deposition kinetic laws in the BCl_3-CH_4-H_2 system.

	γ	δ	Q_{tot}(sccm)	T(°C) 850	900	950	1000
①	5	4	250	78/22 (3.5)	73/26 (2.8)	74/26 (2.8)	-
②		2	390	78/22 (3.6)	75/25 (3.0)	76/24 (3.2)	67/33 (2.0)
③	2	4	390	74/26 (2.9)	75/25 (3.1)	72/28 (2.6)	-
④		2	210	71/29 (2.4)	70/30 (2.3)	74/26 (2.9)	-

Table 4 : B/C atomic ratio of coatings deposited in the BCl_3-CH_4-H_2 system, as measured by AES

Figure captions

Fig. 1: CVD reactor coupled with a FTIR spectrometer for in situ gas phase analysis

Fig. 2: Ternary diagram showing the gas phase composition experimentally investigated in the BCl_3-CH_4-H_2 system (partial pressures are given for a total pressure of 12 kPa).

Fig. 3: Ternary diagram showing the gas phase composition experimentally investigated in the BCl_3-MTS-H_2 system (partial pressures are given for a total pressure of 12 kPa).

Fig. 4: FTIR spectrum of the gas phase in the BCl_3-CH_4-H_2 system for T = 900°C, P = 12kPa, $\delta = 4$, $\gamma = 5$ and Q = 250 sccm

Fig. 5: Variations with temperature of the FTIR peak areas of the various gas species in the BCl_3-CH_4-H_2 system, with (black triangles) and without (open squares) a porous substrate, at P = 12 kPa and (a) $\delta = 4$, $\gamma = 5$, Q = 250sccm, (b) $\delta = 2$, $\gamma = 5$, Q = 390 sccm, (c) $\delta = 4$, $\gamma = 2$, Q = 390 sccm and (d) $\delta = 2$, $\gamma = 2$, Q = 210 sccm.

Fig. 6: Variations with temperature of the FTIR peak areas of the various gas species in the BCl_3-CH_4-H_2 system, with (black triangles) and without (open squares) a porous substrate, at P = 2kPa, $\delta = 4$, $\gamma = 5$ and Q = 250 sccm.

Fig. 7: Influence of the temperature on the calculated yields at homogeneous phase equilibrium in the BCl_3-CH_4-H_2 system, at P = 10 kPa, $\delta = 2$ and $\gamma = 2$.

Fig. 8: FTIR spectrum of the gas phase in the BCl_3-MTS-H_2 system for T = 900°C, P = 12kPa, $\alpha = 12$, $\beta = 1$ and Q = 420 sccm.

Fig. 9: Variations with temperature of the FTIR peak areas of the various gas species in the BCl_3-MTS-H_2 system, with (black triangles) and without (open squares) a porous substrate, at P = 12kPa, $\alpha = 12$, $\beta = 1$ and Q = 420 sccm.

Fig. 10: Variations with temperature of the FTIR peak areas of chlorosilanes and SiCl4, with (dark triangles) and without (open squares) a porous substrate, at P = 12kPa, α = 20, β =0.3 and Q = 365 sccm.

Fig. 11: Variations with temperature of the FTIR peak areas of $HBCl_2$, with (dark triangles) and without (open squares) a porous substrate, at P = 12kPa, α = 20, β =0.3, for (a) Q = 420 sccm and (b) Q = 175 sccm.

Fig. 12: Variations with temperature of the FTIR peak areas of CH_4 and $SiCl_4$, at P = 5kPa, either with BCl_3 (dark triangles, α = 12, β = 1 and Q = 245 sccm) or without BCl_3 (open circles, α = 12).

Fig. 13: Influence of the reciprocal temperature on the deposition rate (Arrhenius plot) in the BCl_3-CH_4-H_2 system, at P = 12kPa and for the various compositions and flow rates of the gas phase.

Fig. 14: Influence of the reciprocal temperature on the deposition rate (Arrhenius plot) in the BCl_3-CH_4-H_2 system, at P = 2 kPa and for δ = 4, γ = 5 and Q = 250 sccm.

Fig. 15: Influence of the reciprocal temperature on the deposition rate (Arrhenius plots) in the BCl_3-MTS-H_2 system, for the various compositions and flow rates of the gas phase, at (a) P = 2kPa, (b) P = 5 kPa and (c) P = 12 kPa.

Fig. 16: Variations with temperature of the elemental composition of the coatings deposited at various pressures and for (a) α = 20, β = 0.3, Q = 243 sccm (P = 2 and 5 kPa) or Q = 365 sccm (P = 12 kPa) and (b) α = 12, β = 1, Q = 245 sccm (P = 2 and 5 kPa) or Q = 420 sccm (P = 12 kPa).

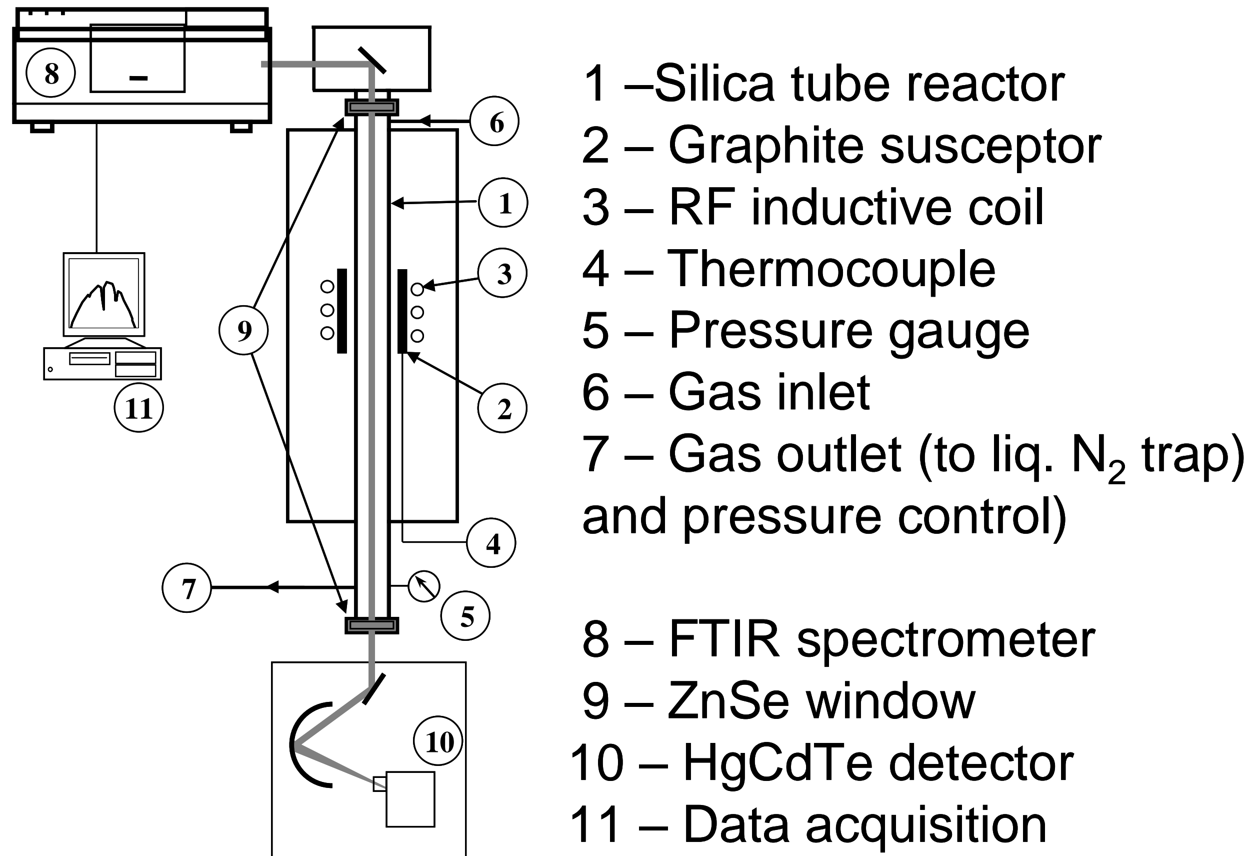

Fig. 1: CVD reactor coupled with a FTIR spectrometer for in situ gas phase

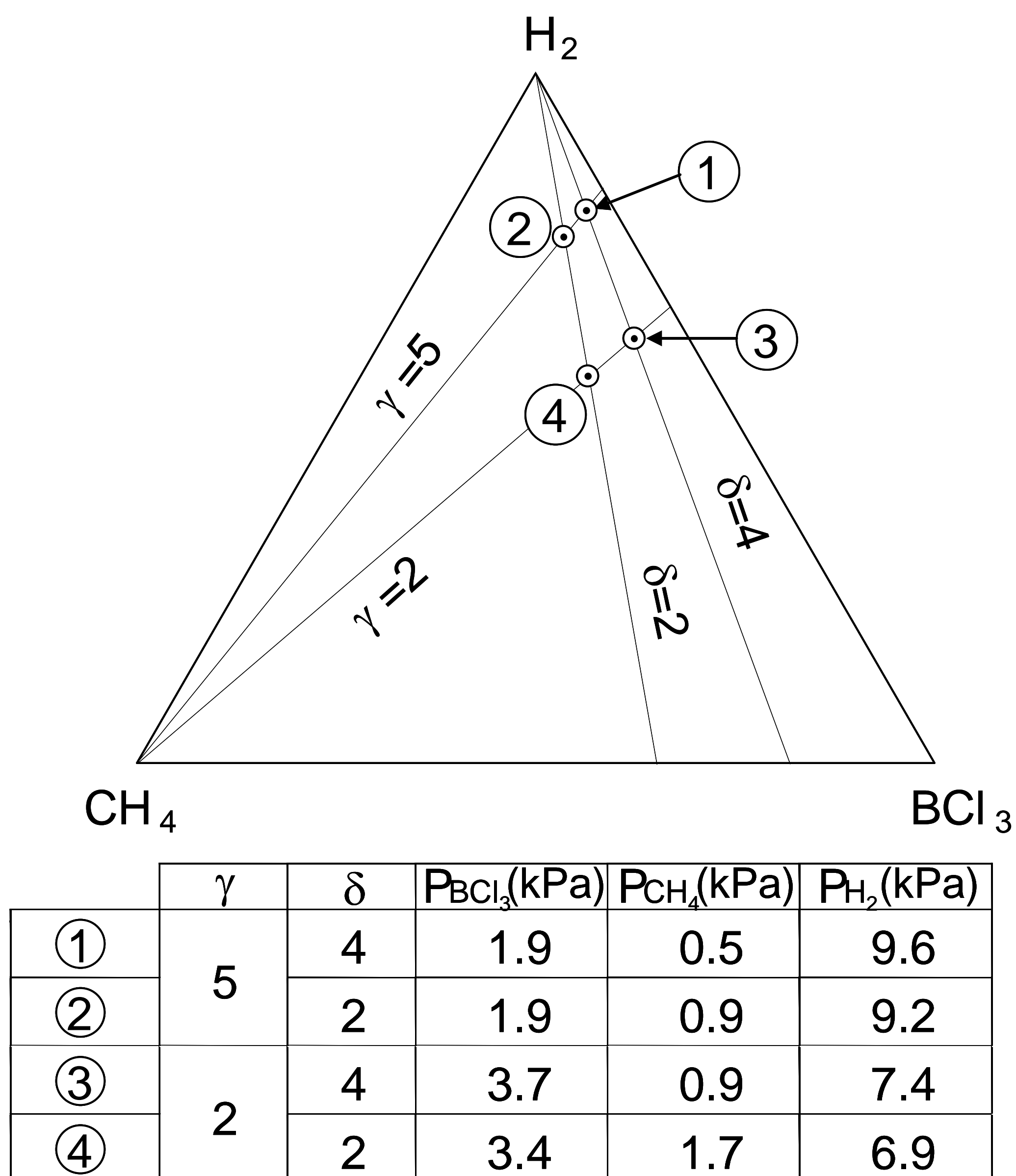

	γ	δ	P_{BCl_3}(kPa)	P_{CH_4}(kPa)	P_{H_2}(kPa)
①	5	4	1.9	0.5	9.6
②		2	1.9	0.9	9.2
③	2	4	3.7	0.9	7.4
④		2	3.4	1.7	6.9

Fig. 2: Ternary diagram showing the gas phase composition experimentally investigated in the BCl_3-CH_4-H_2 system (partial pressures are given for a total pressure of 12 kPa).

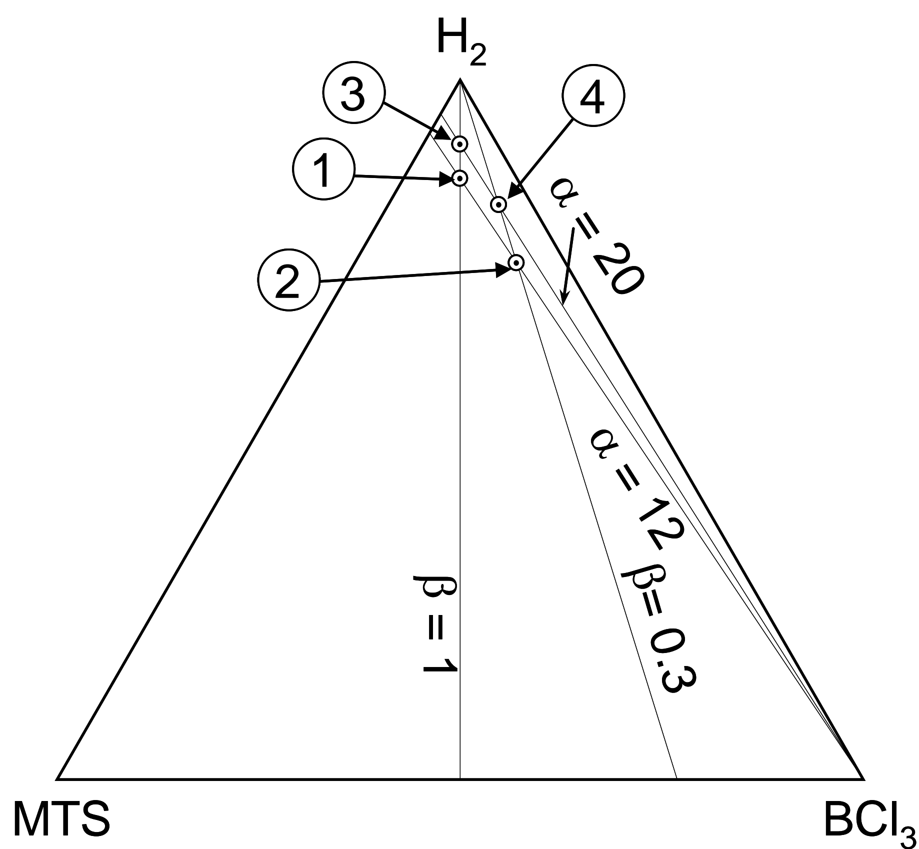

	α	β	P_{BCl_3}(kPa)	P_{MTS}(kPa)	P_{H_2}(kPa)
①	12	1	0.85	0.85	10.3
②		0.3	2.5	0.7	8.8
③	20	1	0.55	0.55	10.9
④		0.3	1.6	0.5	9.9

Fig. 3: Ternary diagram showing the gas phase composition experimentally investigated in the BCl_3-MTS-H_2 system (partial pressures are given for a total pressure of 12 kPa).

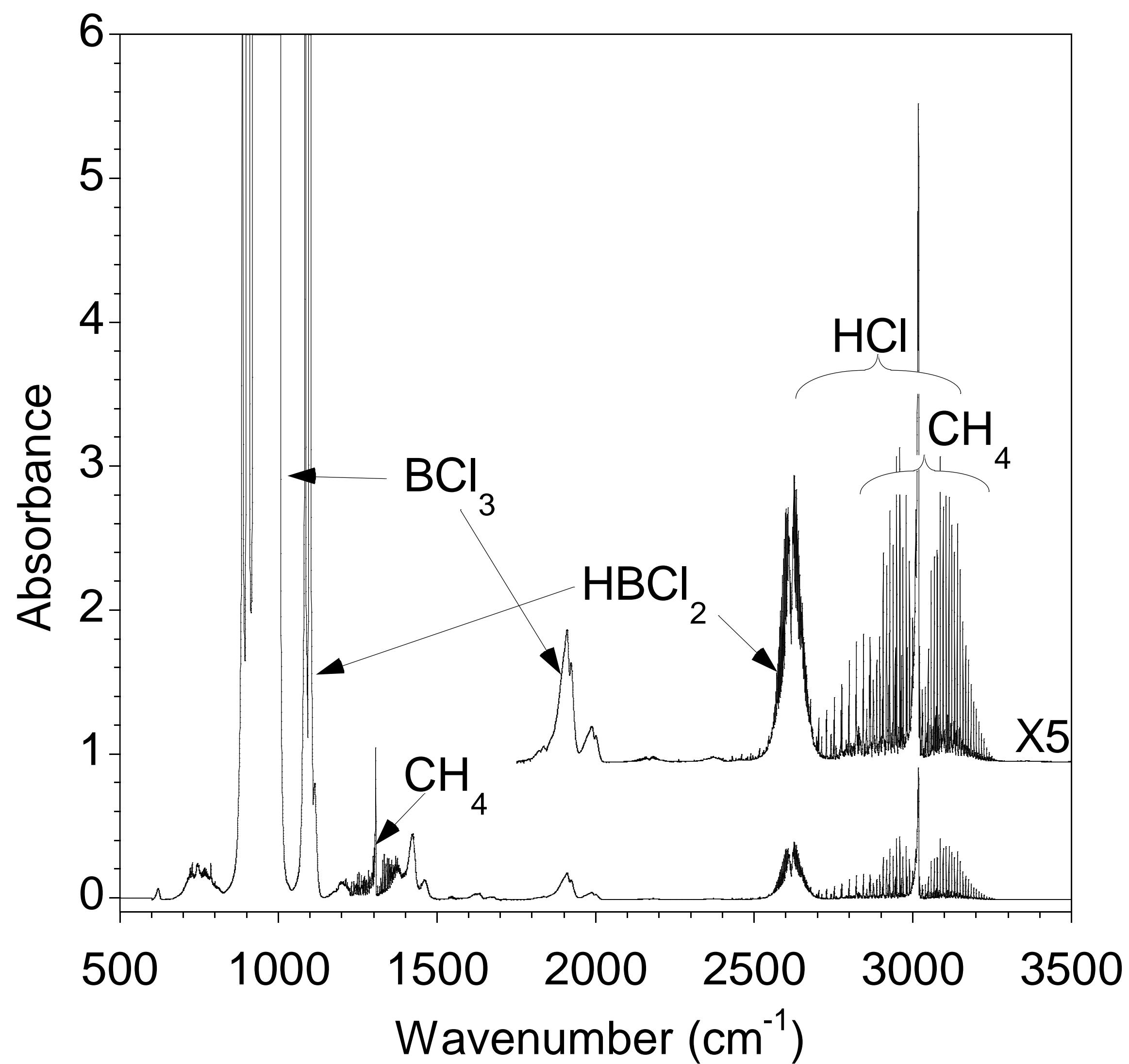

Fig. 4: FTIR spectrum of the gas phase in the BCl_3-CH_4-H_2 system for T = 900°C, P = 12kPa, δ = 4, γ =5 and Q = 250 sccm

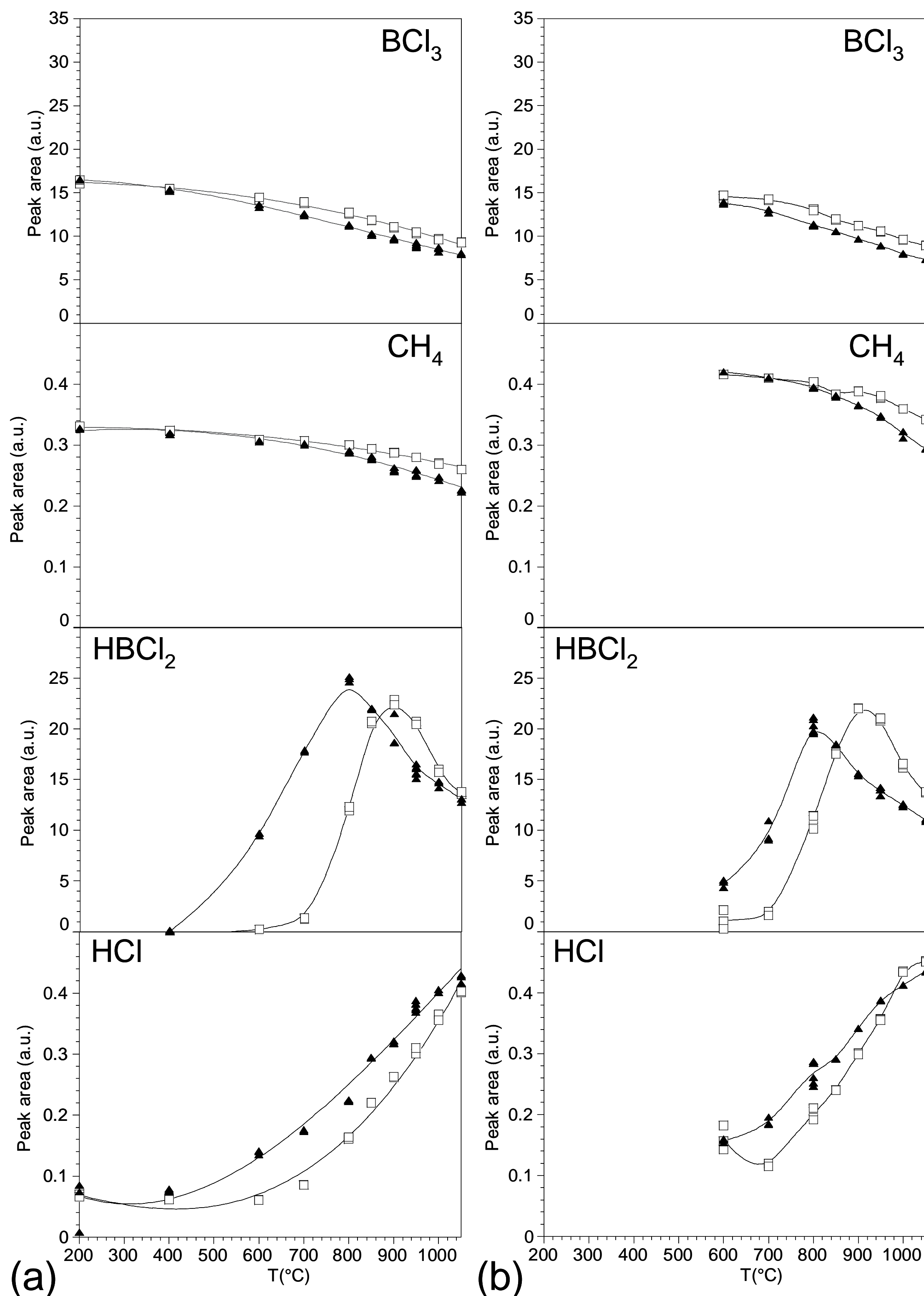

Fig. 5: Variations with temperature of the FTIR peak areas of the various gas species in the BCl_3-CH_4-H_2 system, with (black triangles) and without (open squares) a porous substrate, at P = 12 kPa and (a) $\delta = 4$, $\gamma = 5$, Q = 250sccm, (b) $\delta = 2$, $\gamma = 5$, Q = 390 sccm, (c) $\delta = 4$, $\gamma = 2$, Q = 390 sccm and (d) $\delta = 2$, $\gamma = 2$, Q = 210 sccm.

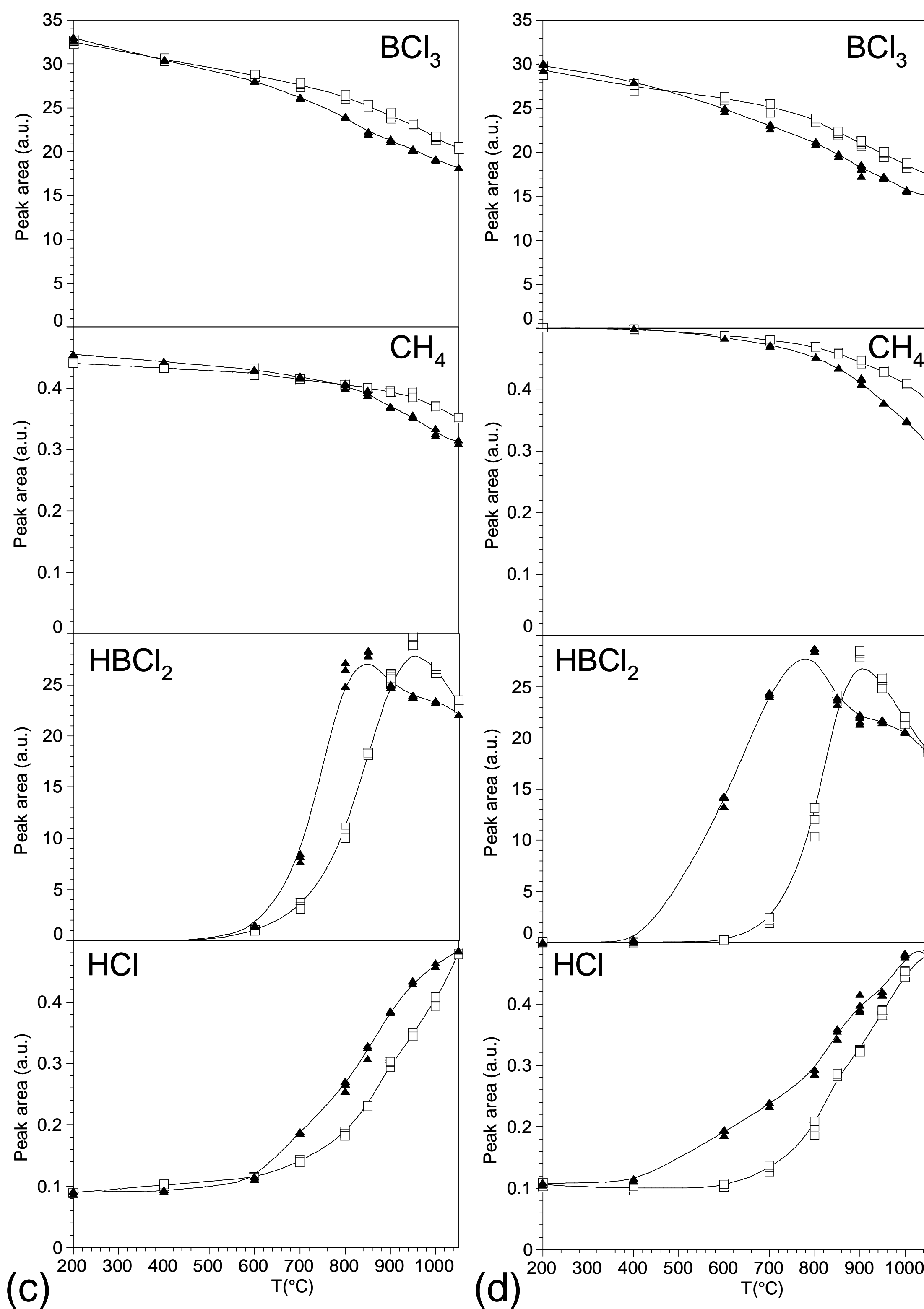

Fig. 5: Variations with temperature of the FTIR peak areas of the various gas species in the BCl_3-CH_4-H_2 system, with (black triangles) and without (open squares) a porous substrate, at P = 12 kPa and (a) $\delta = 4$, $\gamma = 5$, Q = 250sccm, (b) $\delta = 2$, $\gamma = 5$, Q = 390 sccm, (c) $\delta = 4$, $\gamma = 2$, Q = 390 sccm and (d) $\delta = 2$, $\gamma = 2$, Q = 210 sccm.

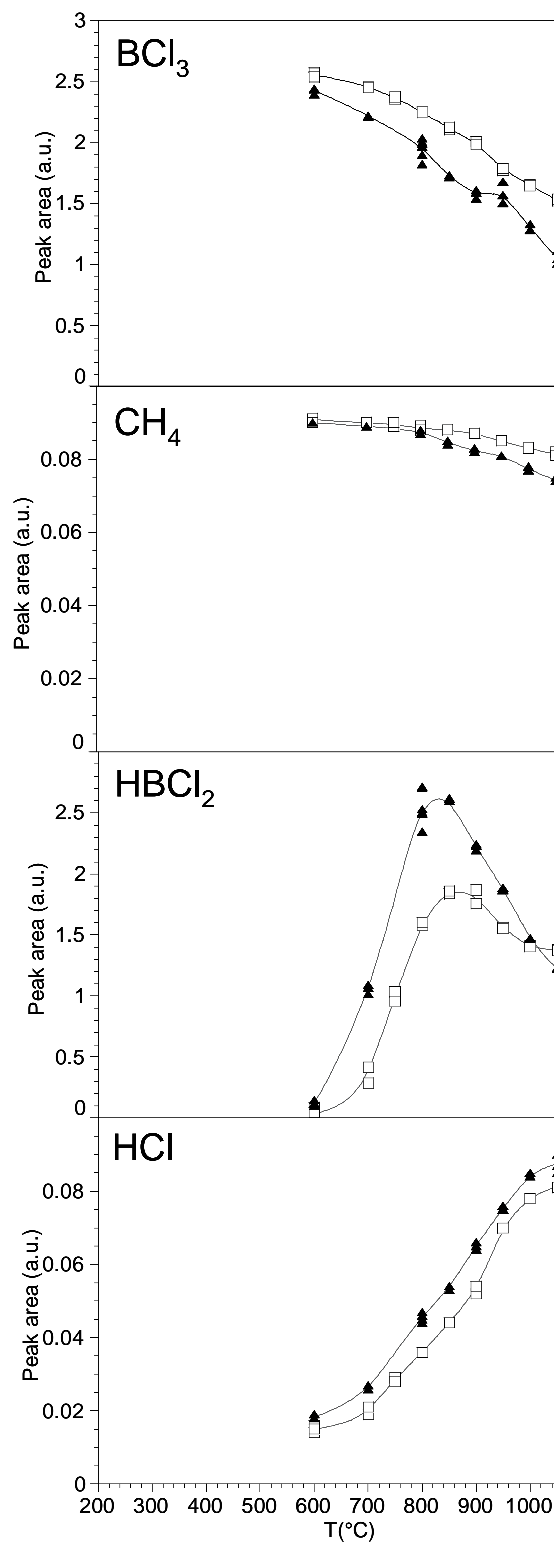

Fig. 6: Variations with temperature of the FTIR peak areas of the various gas species in the BCl_3-CH_4-H_2 system, with (black triangles) and without (open squares) a porous substrate, at P = 2kPa, $\delta = 4$, $\gamma = 5$ and Q = 250 sccm.

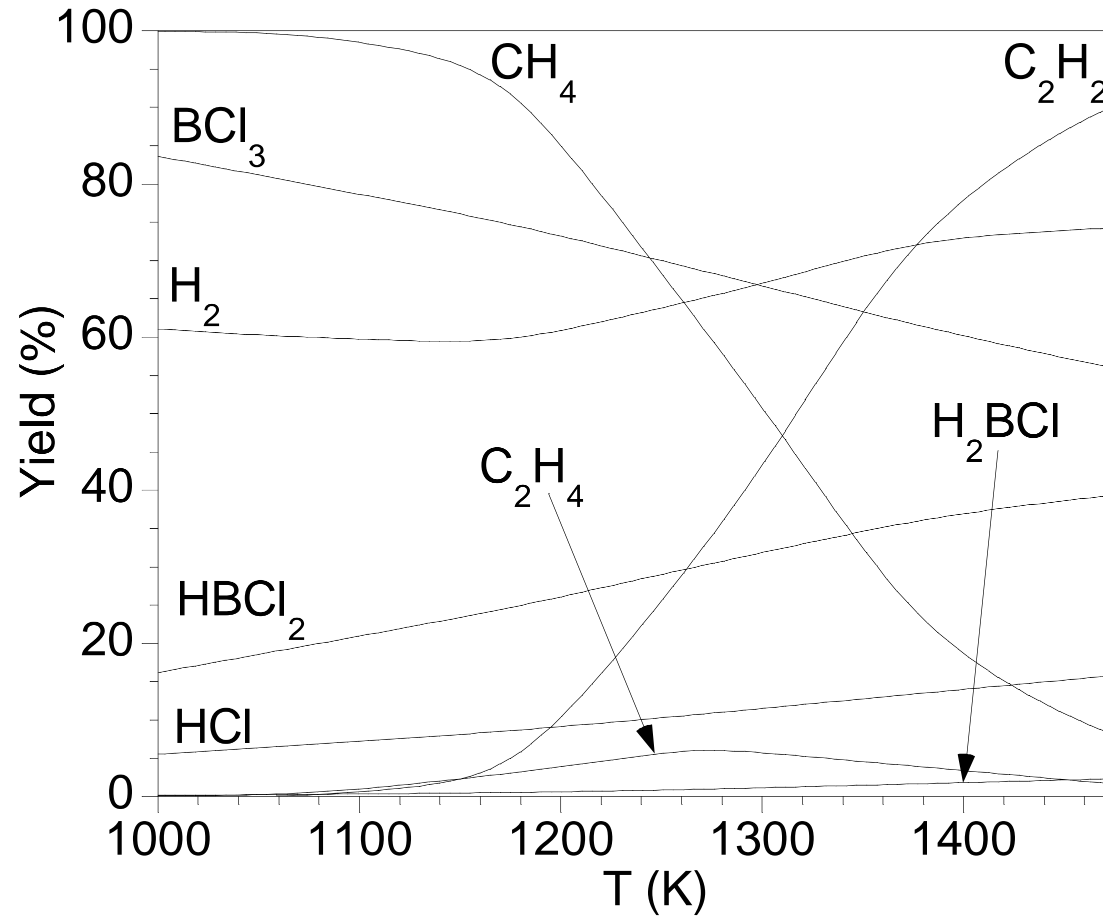

Fig. 7: Influence of the temperature on the calculated yields at homogeneous phase equilibrium in the BCl_3-CH_4-H_2 system, at P = 10 kPa, δ = 2 and γ =2.

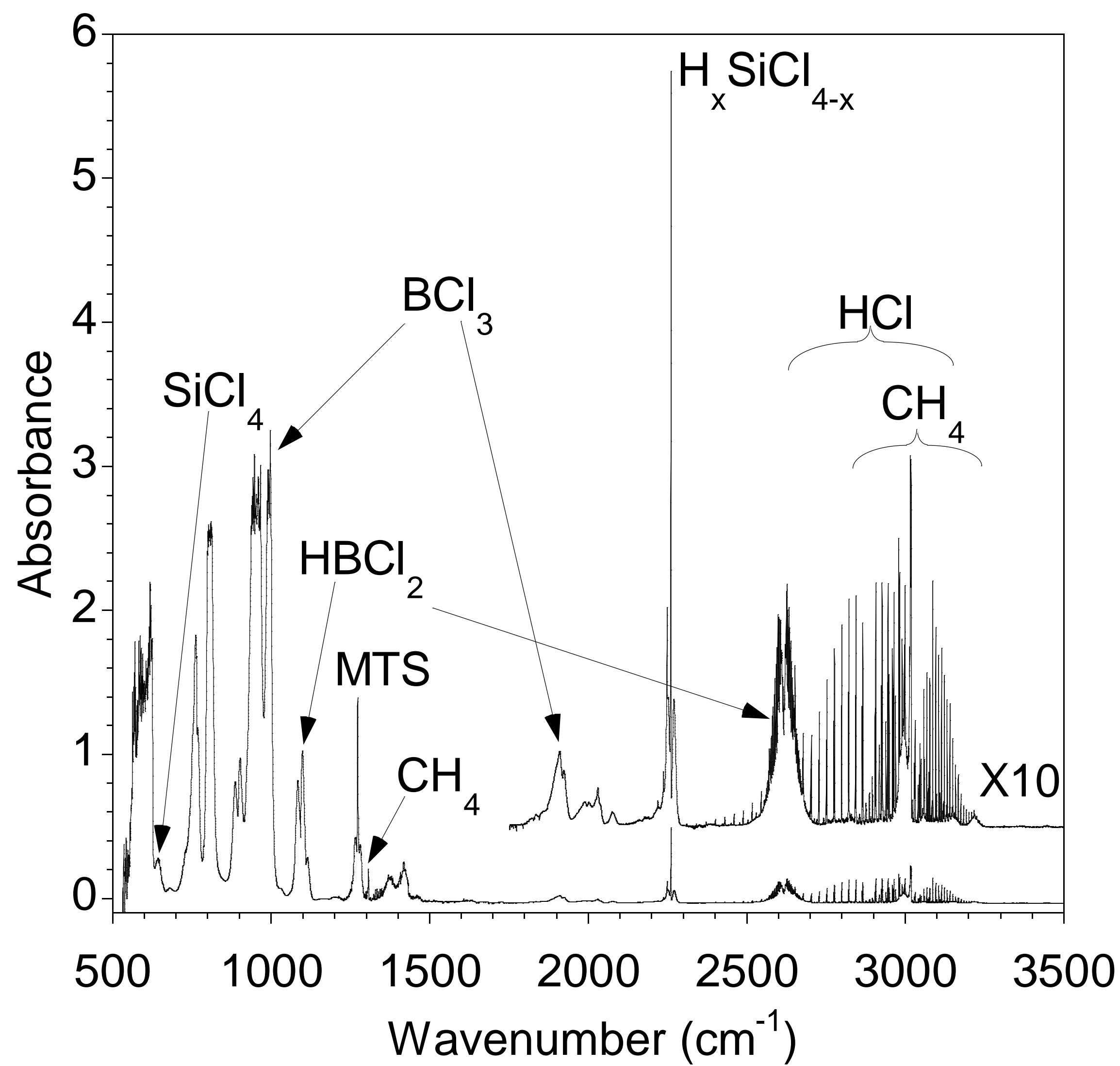

Fig. 8: FTIR spectrum of the gas phase in the BCl_3-MTS-H_2 system for T = 900°C, P = 12kPa, α = 12, β =1 and Q = 420 sccm.

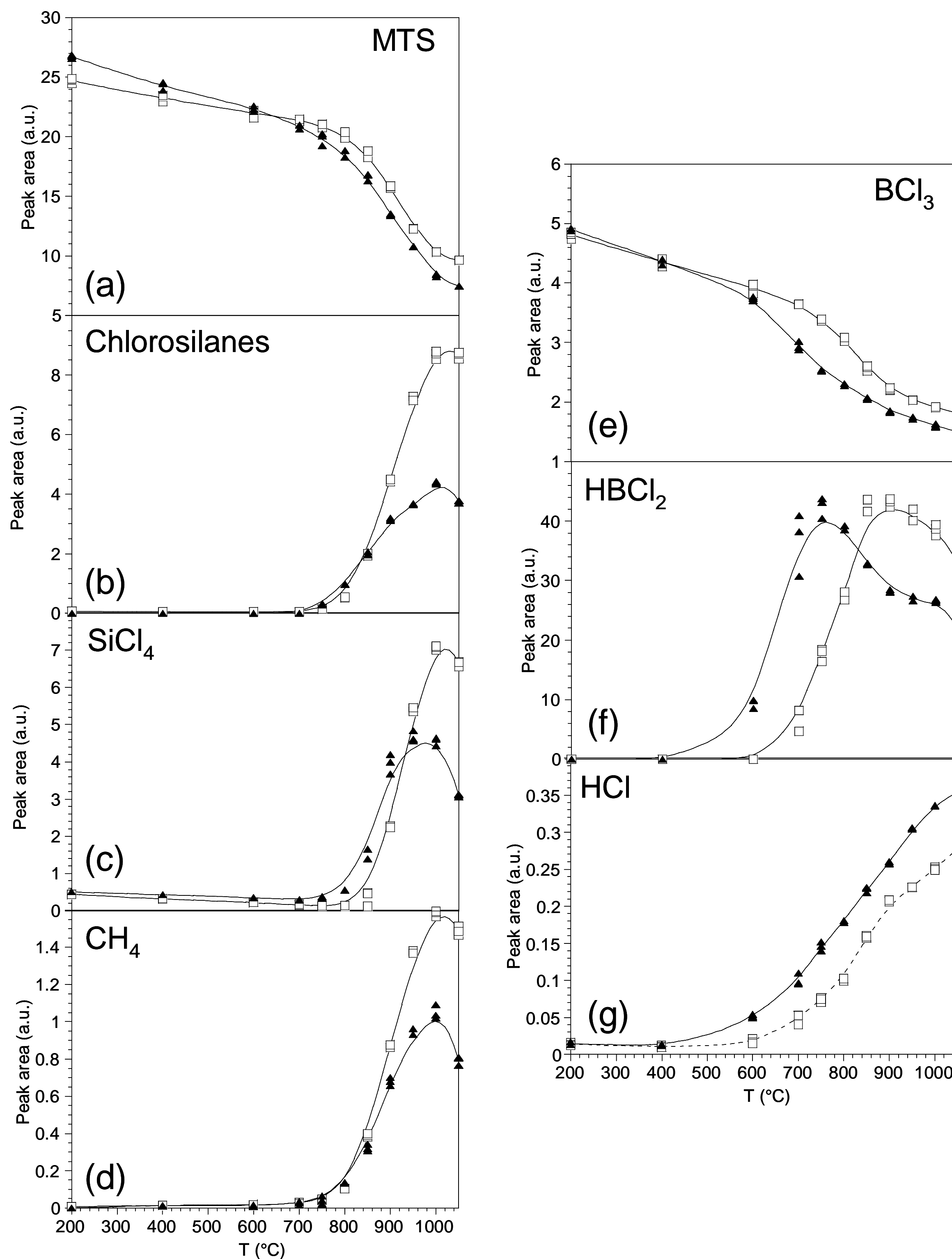

Fig. 9: Variations with temperature of the FTIR peak areas of the various gas species in the BCl_3-MTS-H_2 system, with (black triangles) and without (open squares) a porous substrate, at P = 12kPa, α = 12, β =1 and Q = 420 sccm.

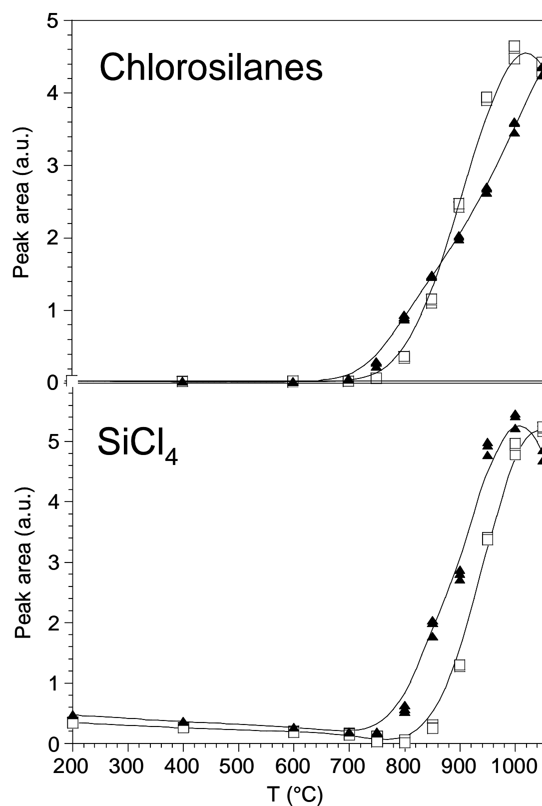

Fig. 10: Variations with temperature of the FTIR peak areas of chlorosilanes and SiCl4, with (dark triangles) and without (open squares) a porous substrate, at P = 12kPa, $\alpha = 20$, $\beta = 0.3$ and Q = 365 sccm.

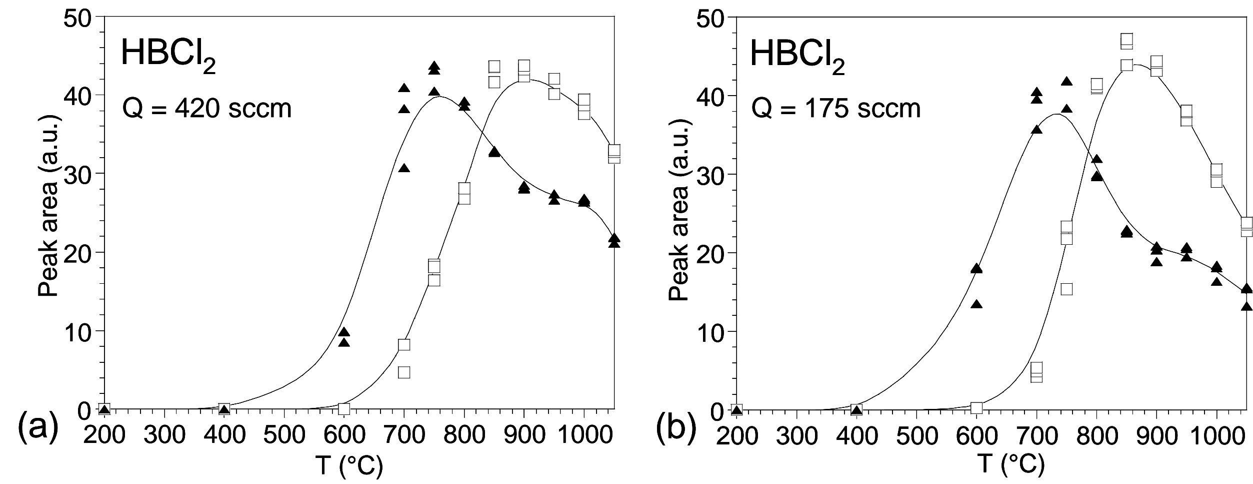

Fig. 11: Variations with temperature of the FTIR peak areas of $HBCl_2$, with (dark triangles) and without (open squares) a porous substrate, at P = 12kPa, $\alpha = 20$, $\beta = 0.3$, for (a) Q = 420 sccm and (b) Q = 175 sccm.

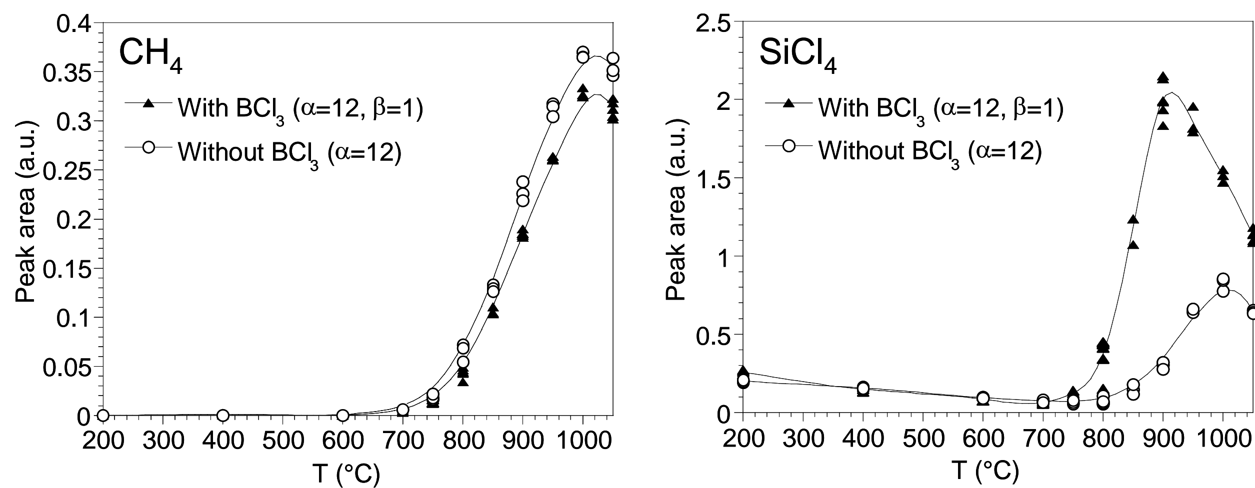

Fig. 12: Variations with temperature of the FTIR peak areas of CH_4 and $SiCl_4$, at P = 5kPa, either with BCl_3 (dark triangles, $\alpha = 12$, $\beta = 1$ and Q = 245 sccm) or without BCl_3 (open circles, $\alpha = 12$).

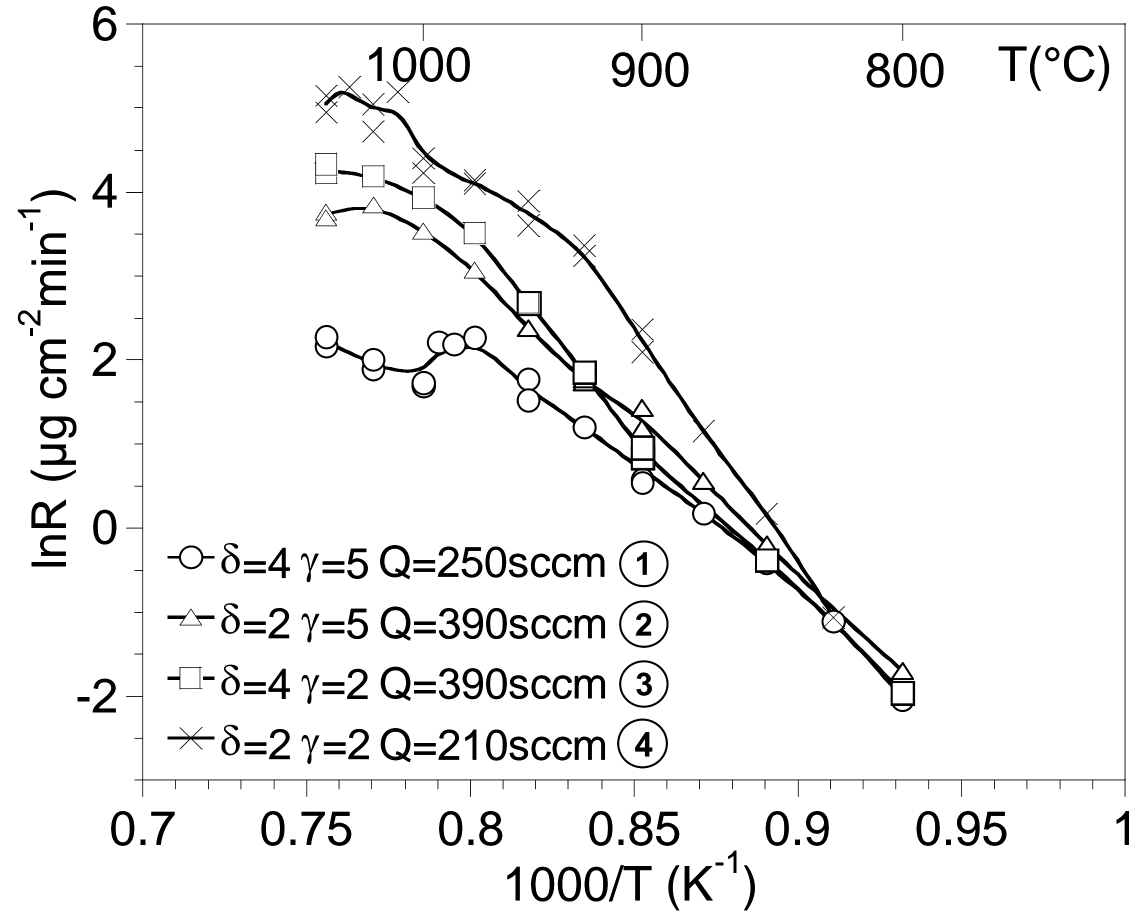

Fig. 13: Influence of the reciprocal temperature on the deposition rate (Arrhenius plot) in the BCl_3-CH_4-H_2 system, at P = 12kPa and for the various compositions and flow rates of the gas phase.

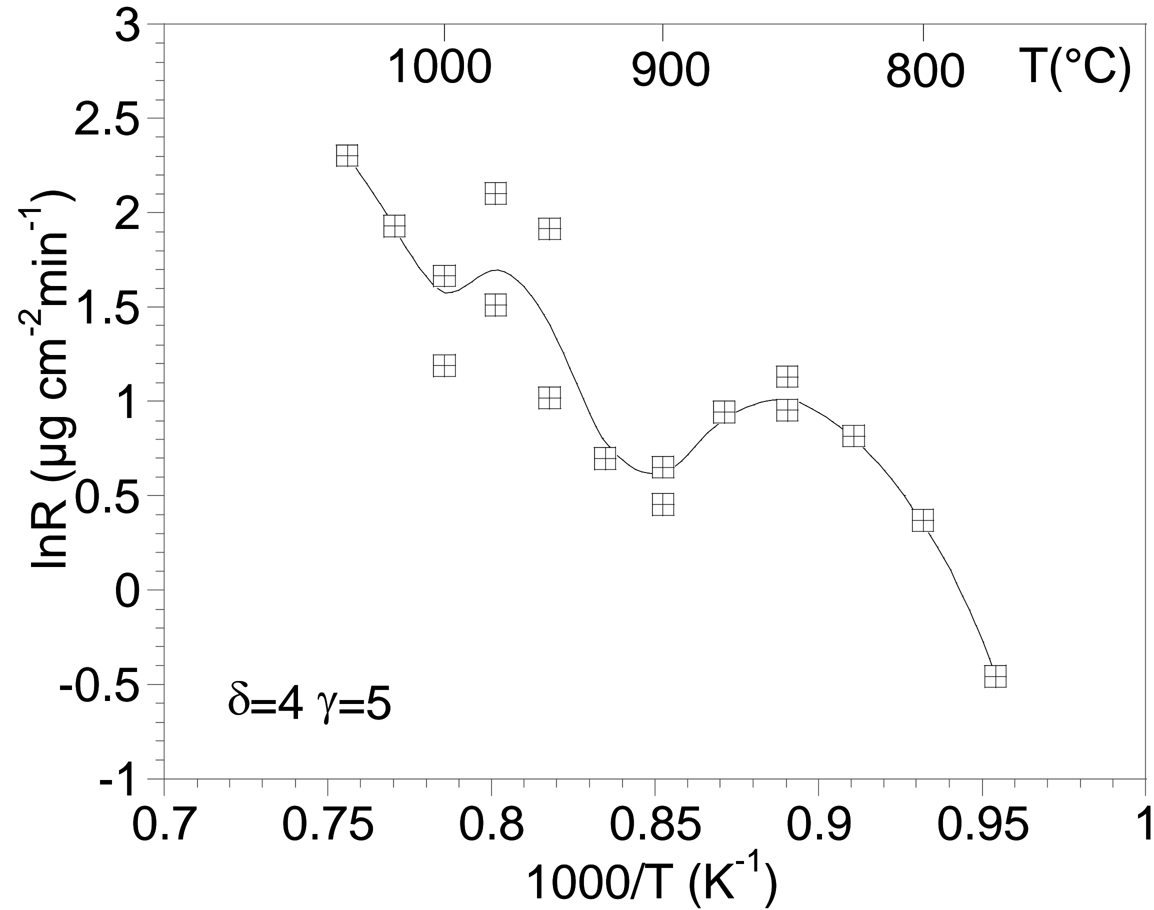

Fig. 14: Influence of the reciprocal temperature on the deposition rate (Arrhenius plot) in the BCl_3-CH_4-H_2 system, at P = 2 kPa and for $\delta = 4$, $\gamma = 5$ and Q = 250 sccm.

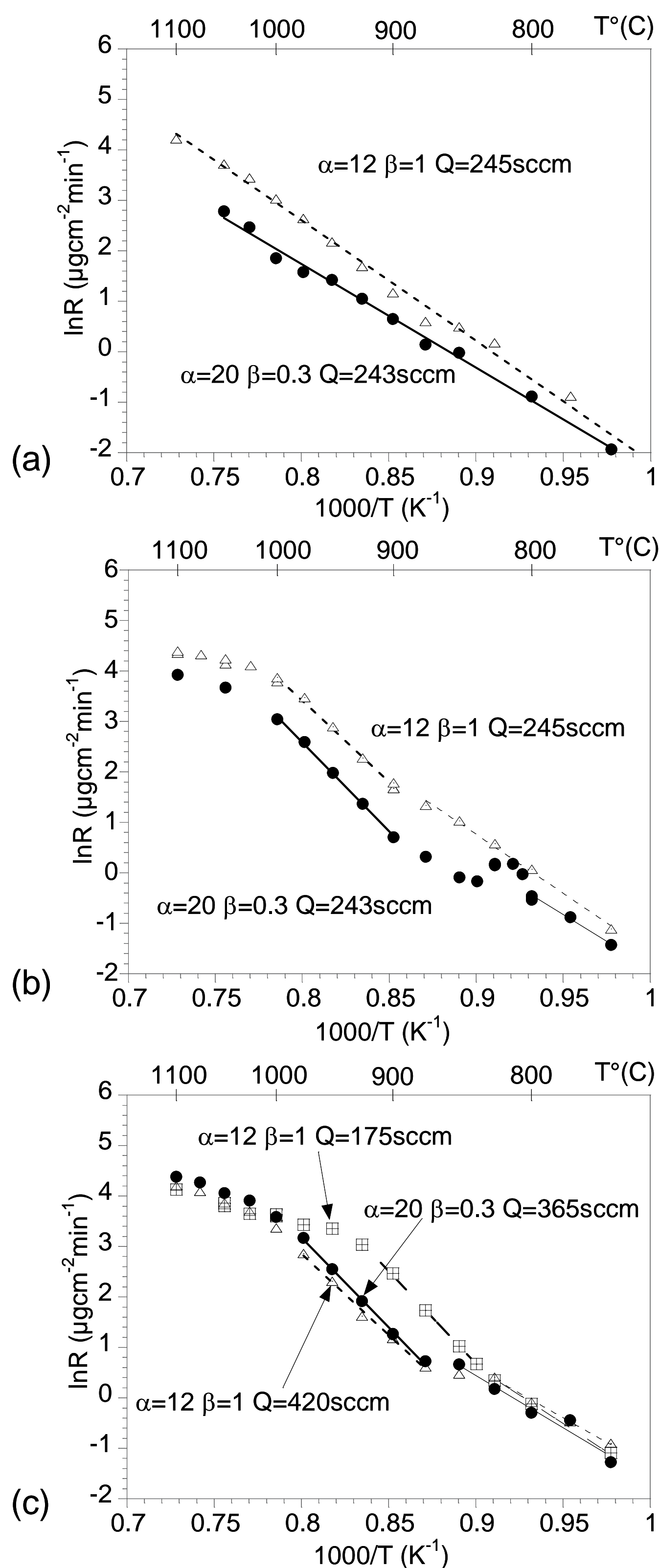

Fig. 15: Influence of the reciprocal temperature on the deposition rate (Arrhenius plots) in the BCl_3-MTS-H_2 system, for the various compositions and flow rates of the gas phase, at (a) P = 2kPa, (b) P = 5 kPa and (c) P = 12 kPa.

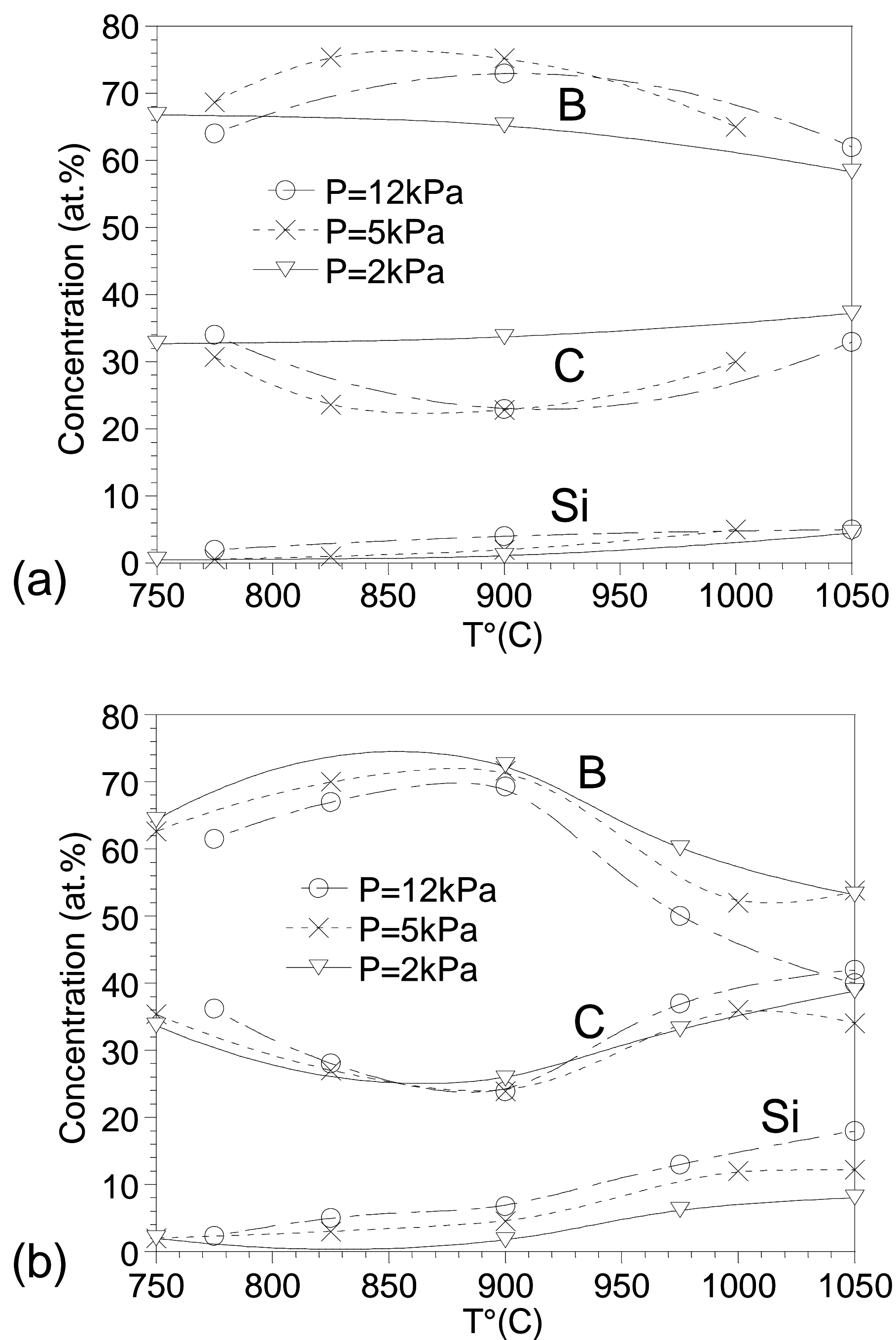

Fig. 16: Variations with temperature of the elemental composition of the coatings deposited at various pressures and for (a) $\alpha = 20$, $\beta = 0.3$, Q = 243 sccm (P = 2 and 5 kPa) or Q = 365 sccm (P = 12 kPa) and (b) $\alpha = 12$, $\beta = 1$, Q = 245 sccm (P = 2 and 5 kPa) or Q = 420 sccm (P = 12 kPa).